Geophysical Research Letters

RESEARCH LETTER
10.1029/2023GL107346

Divergence in Autumn Phenology Extracted From Different Satellite Proxies Reveals the Timetable of Leaf Senescence Over Deciduous Forests

Cong Wang[1], Yajie Yang[2], Gaofei Yin[2], Qiaoyun Xie[3], Baodong Xu[4], Aleixandre Verger[5,6,7], Adrià Descals[6,7], Iolanda Filella[6,7], and Josep Peñuelas[6,7]

[1]Key Laboratory for Geographical Process Analysis & Simulation of Hubei Province, School of Urban and Environmental Sciences, Central China Normal University, Wuhan, China, [2]Faculty of Geosciences and Environmental Engineering, Southwest Jiaotong University, Chengdu, China, [3]School of Engineering, The University of Western Australia, Perth, WA, Australia, [4]Macro Agriculture Research Institute, College of Resource and Environment, Huazhong Agricultural University, Wuhan, China, [5]CIDE, CSIC-UV-GV, Valèncía, Spain, [6]CREAF, Barcelona, Spain, [7]CSIC, Global Ecology Unit CREAF-CSIC-UAB, Barcelona, Spain

Abstract Remote sensing detection of autumn phenology is challenging and highly uncertain, as exemplified by the observed divergence in autumn phenology extracted from different proxies. Here, we compared the autumn phenology derived from Solar-Induced chlorophyll Fluorescence (SIF), Chlorophyll/Carotenoid Index (CCI), Enhanced Vegetation Index (EVI), and Normalized Difference Vegetation Index (NDVI) over deciduous forest sites. We observed a clear temporal sequence in the derived autumn phenology from various proxies: SIF < CCI < EVI < NDVI. Comparison with field measurements supported that SIF, EVI, and NDVI can successfully capture the attenuation of photosynthetic activity, leaf coloration, and leaf fall, respectively. The sequence among the autumn phenology derived from those proxies was also consistent with their responses to climate cues, where SIF had the highest partial correlation coefficient to solar radiation in autumn, followed by CCI, EVI, and NDVI, while NDVI was more correlated with temperature, followed by EVI, CCI, and SIF.

Plain Language Summary The autumn phenology of deciduous forests is critical for estimating carbon sequestration and understanding the responses of vegetation to climate change. However, the autumn phenology metrics derived from different satellite proxies show high discrepancies. Here, we hypothesized that leaf senescence of deciduous forests is a progressive process, and that the different satellite proxies capture different stages of this timetable. To test this hypothesis, we compared the autumn phenology of deciduous forests derived from Solar-Induced chlorophyll Fluorescence (SIF), Chlorophyll/Carotenoid Index (CCI), Enhanced Vegetation Index (EVI), and Normalized Difference Vegetation Index (NDVI). We revealed the timetable of autumn phenology derived from different satellite proxies, that is, SIF-based autumn phenology is the earliest, followed by CCI-based, EVI-based, and NDVI-based autumn phenology, which had a close relationship with their responses to temperature and solar radiation in autumn. Comparison with field measurements supported that SIF, EVI, and NDVI can successfully capture the attenuation of photosynthetic activity, leaf coloration, and leaf fall, respectively, which occur in sequence during the leaf senescence process. These findings improved our understanding on the meaning of remote sensing derived autumn phenology, and will contribute to the accurate estimation of the length of photosynthetic active season.

Key Points:

- The sequence among the autumn phenology derived from satellite proxies is Solar-Induced chlorophyll Fluorescence (SIF) < Chlorophyll/Carotenoid Index (CCI) < Enhanced Vegetation Index (EVI) < Normalized Difference Vegetation Index (NDVI)
- SIF, CCI, EVI, and NDVI capture different stages of senescence of deciduous forests
- This sequence among autumn phenology derived from SIF, CCI, EVI, and NDVI is consistent with their responses to climate cues

Supporting Information:

Supporting Information may be found in the online version of this article.

Correspondence to:

G. Yin,
yingf@swjtu.edu.cn

Citation:

Wang, C., Yang, Y., Yin, G., Xie, Q., Xu, B., Verger, A., et al. (2024). Divergence in autumn phenology extracted from different satellite proxies reveals the timetable of leaf senescence over deciduous forests. *Geophysical Research Letters*, *51*, e2023GL107346. https://doi.org/10.1029/2023GL107346

Received 15 NOV 2023
Accepted 26 JAN 2024

1. Introduction

Deciduous forests account for approximately a half of the terrestrial surface forests and offset massive anthropogenic CO_2 emissions (Bonan, 2008; Le Quere et al., 2009). The autumn phenology of deciduous forests marks the transition of plant growth from the active to the dormant stages (Estiarte & Penuelas, 2015), and is a critical factor determining the length of growing season and carbon sequestration (Richardson et al., 2010; Wu et al., 2013). Accurate characterization of autumn phenology is therefore necessary for understanding seasonal carbon, water, and energy cycles of ecosystems and revealing the response of forests to climate change (Bonan, 2008; Gallinat et al., 2015; Zheng et al., 2002).

Remote sensing is currently the only feasible way to support the extraction of vegetation phenology on a large scale. The satellite-based Vegetation Indices (VIs), for example, the Normalized Difference Vegetation Index

(NDVI), and Enhanced Vegetation Index (EVI), are the most widely used VIs employed to derive phenological metrics, which tend to characterize the canopy greenness/structural changes (Gamon et al., 1995; Huete et al., 2002; Myneni et al., 1995). Different from those greenness/structural VIs, physiological vegetation variables are not limited to monitor changes in visible leaf color and amount, but also changes in the intrinsic photosynthetic activities of vegetation (Wu et al., 2013). The Chlorophyll/Carotenoid Index (CCI), representing the seasonal changes in chlorophyll/carotenoid pigment ratios (Penuelas et al., 1994; Wong & Gamon, 2015), is strongly correlated with the composition of the pigment pool, specifically the chlorophyll/carotenoid ratio (Gamon et al., 2016; Wong et al., 2019; Yin et al., 2020), which is an important determiner of light-use efficiency and ultimately influences photosynthesis (Croft et al., 2017). Besides, the Solar-Induced chlorophyll Fluorescence (SIF), representing the signal emitted by green plants when solar photons are absorbed by chlorophylls within photosynthetic machinery (Porcar-Castell et al., 2014), provides insights to estimate phenology from the canopy photosynthetic (physiological) perspective (Jeong et al., 2017; Lu et al., 2018; Walther et al., 2016).

Remote sensing detection of autumn phenology (i.e., End of growing Season, EOS) is challenging and highly uncertain (Elmore et al., 2012; Ganguly et al., 2010; Guyon et al., 2011), as exemplified by the observed divergence in EOS extracted from different proxies (Lu et al., 2018; X. Wang et al., 2020). Recent studies revealed that EOS extracted from SIF was significantly different with that extracted from EVI or NDVI for deciduous forests in the Northern Hemisphere. For example, Walther et al. (2016) presented that SIF-based EOS was significantly earlier than the green biomass changing period proxied by EVI or NDVI for northern forests, but was consistent with Gross Primary Production (GPP)-based one. A similar phenomenon was also reported by Yin et al. (2020): CCI-derived EOS was much earlier than the ones from EVI or NDVI for both deciduous forest and evergreen coniferous forests, which has been proved to have the capability of detecting photosynthetic autumn phenology proxied by GPP (Gamon et al., 2016; Yin et al., 2020, 2022). However, the differences between SIF and CCI in extracting EOS of deciduous forests have not been explored, and the mechanisms underlying the divergence in EOS extracted from different proxies are still elusive.

Recently, field measurements indicate that leaf senescence over deciduous forests is a progressive process following a specific timetable, for example, leaf nutrient relocation, chlorophyll degradation, leaf coloration and leaf shedding (Marien et al., 2019). It is currently unclear which specific stages of leaf senescence can be captured through the extraction of autumn phenology information from different satellite proxies. In this study, we compared the autumn phenology extracted from different satellite-based proxies, that is, SIF, CCI, EVI, and NDVI. The phenology extracted from continuous flux tower-based GPP time series and field observations of autumn phenophases over deciduous forest sites were employed as a reference to validate the satellite metrics. Finally, we analyzed the climatic factors determining the autumn phenology from different satellite proxies. This work highlighted the divergent autumn phenology extracted from different satellite proxies and their relationship with filed-observed phenological process, improving our understanding for interpretation of land surface phenology as well as their responses to climate clues, which will in turn promote satellite-based autumn phenology applications in different usage scenarios.

2. Materials and Methods

2.1. Remote Sensing Data Sets

2.1.1. GOSIF Product

The GOSIF (Global OCO-2 SIF) is a global spatio-temporal continuous SIF product at 0.05° and 8-day resolution available from 2001 to present (Li & Xiao, 2019). It was derived with a machine learning algorithm trained with Orbiting Carbon Observatory-2 (OCO-2) SIF and using Moderate Resolution Imaging Spectroradiometer (MODIS) vegetation data and meteorological reanalysis data as inputs. The data sets had a good performance validated by original SIF observations (Root Mean Square Error [RMSE] = 0.07 W m^{-2} μm^{-1} sr^{-1}) and had been widely applied for autumn phenology extraction over large scales (Ren et al., 2021; C. Wang et al., 2022; J. Zhang et al., 2022).

2.1.2. Vegetation Indices

The NDVI, EVI and CCI were calculated as:

$$\mathrm{NDVI} = \frac{B_2 - B_1}{B_2 + B_1} \quad (1)$$

$$\mathrm{EVI} = \frac{2.5(B_2 - B_1)}{B_2 + 6B_1 - 7.5B_3 + 1} \quad (2)$$

$$\mathrm{CCI} = \frac{B_{11} - B_1}{B_{11} + B_1} \quad (3)$$

where B_1, B_2, B_3, and B_{11} are the MODIS surface reflectances in bands 1 (620–670 nm), 2 (841–876 nm), 3 (459–479 nm), and 11 (526–536 nm), respectively.

We used the MCD19A1 Version 6 product which provides daily surface reflectance for MODIS bands 1–12 at a spatial resolutions of 1 km. This product was generated using the Multi-Angle Implementation of Atmospheric Correction algorithm, which used an adaptive time series and spatial analysis to derive atmospheric aerosol concentration and surface reflectance without empirical assumptions (Lyapustin et al., 2012). Pixels contaminated by cloud, snow or a high aerosol optical depth were excluded based on the layer of quality assurance of the data set. Data with viewing zenith angles >45° were also excluded to minimize the effects of the bidirectional reflectance distribution function (BRDF) (Middleton et al., 2016; R. Wang et al., 2020). Finally, the daily CCI, EVI, and NDVI were composited at 8-day period by computing the mean of all valid observations within the 8-day period to match the temporal resolution of the GOSIF products.

2.1.3. MODIS Land Cover Map

We utilized the MODIS Terra and Aqua Combined Land Cover Version 6 data product (MCD12Q1) to screen representative deciduous forest sites. This product provides global land cover types at yearly intervals and 500 m spatial resolution, which is derived using supervised classifications of MODIS Terra and Aqua reflectance data. The Annual International Geosphere-Biosphere Programme classification schemes was chosen in this study, including 11 natural vegetation classes, 3 developed and mosiacked land classes, and three non-vegetated land classes.

2.2. Ground Observations

2.2.1. In Situ GPP Measurements

In-situ GPP measurements were also used to extract autumn phenology, which provided a benchmark for the comparison among the satellite proxies. We obtained GPP measurements of deciduous forest sites from the FLUXNET-2015 data set. The GPP in the FLUXNET-2015 data set was provided by using gap-filled data for net ecosystem exchange and the daytime flux-partitioning method (Pastorello et al., 2020). Sites were selected based on the following criteria: (a) latitudes > 30°N; (b) at least one year of the observations were valid after 2001; and (c) the fraction of deciduous and mixed forests in a 0.05° × 0.05° area surrounding the sampled site was more than 80% based on MODIS Land Cover Map. Detailed information for selected flux-tower-based GPP sites can be found in Table S1 in Supporting Information S1.

2.2.2. Phenological Field Observations

We used field observations of the "colored leaves" and "leaves falling" phenophases from the United States of America National Phenology Network. Sites were selected based on the following criteria: (a) latitudes > 30° N; (b) at least one year of both "colored leaves" and "leaves falling" observations were valid after 2001; and (c) the fraction of deciduous and mixed forests in a 0.05° × 0.05° area surrounding the sampled site was more than 80% based on MODIS Land Cover Map. Detailed information for selected field phenology observation sites can be found in Table S2 in Supporting Information S1. For comparison with satellite derived EOS, we averaged the timing when 50% colored leaves occurred for all deciduous species. The same processing method was also conducted for the item of "leaves falling."

2.3. Reanalysis Climate Data Set

The relationship between satellite-derived autumn phenology and climate cues was implemented to disentangle the underlying mechanisms of the divergent autumn phenology from different proxies. Considering that light and temperature are the main cues controlling leaf senescence in deciduous species in mid- and high-latitude of the Northern Hemisphere (Figure S1 in Supporting Information S1), we employed the downward surface solar radiation and 2-m temperature to represent the environmental cues (Descals et al., 2022; Y. Zhang et al., 2020). This data set was obtained from the ERA5-Land data set at 0.1° and one-hour resolutions, which was developed by the Copernicus Climate Change Service at the European Centre for Medium-Range Weather Forecasts (Munoz-Sabater et al., 2021). For comparison purposes, we integrated the hourly shortwave radiation and temperature data sets to 8-day intervals, and adopted the partial correlation analysis between time series of vegetation variables (i.e., SIF, CCI, EVI, NDVI, and GPP) and climate data. The time series over all selected flux-tower-based GPP sites (Table S1 in Supporting Information S1) were used to illustrate the partial correlation between autumn phenology and climate cues.

2.4. Autumn Phenology Extraction

The satellite-based autumn phenology was extracted from the SIF, CCI, EVI, and NDVI time series through three main steps: (a) *Gap filling*. In winter time, the missing values contaminated by snow were replaced with snow-free background values, which were calculated at pixel level by the average of valid values during the period when GPP was lower than 5% of the annual magnitude. If the GPP measurements were not available at USA NPN sites, the missing values contaminated by snow were replaced with the lower quartile of valid values in November and March. During the growing season, linear interpolation was conducted to fill the missing values such as the cases that were filtered out due to clouds or BRDF effects. (b) *Curve fitting*. A double logistic function was fitted to the smoothed and snow corrected time series to produce continuous curves. The double logistic was suited for phenological monitoring of forests, as it allows asymmetry in the temporal evolution of spring and autumn (Elmore et al., 2012). The double logistic function is as follows:

$$V(t) = V_{\mathrm{min}a} + \frac{V_{\max} - V_{\mathrm{min}a}}{1 + e^{-S_a \cdot (t - T_{mida})}} + \frac{V_{\max} - V_{\mathrm{min}b}}{1 + e^{-S_b \cdot (t - T_{midb})}} \quad (4)$$

where $V(t)$ is the value of vegetation proxy at the day of the year t, $V_{\max}$ is the maximum value during the year, V_{mina} and V_{minb}, are the minimum value of the curve in greenup and senescence, respectively, T_{mida} and T_{midb} are the DOYs of maximum slope of the curve in greenup and senescence, respectively, whereas S_a and S_b are the slopes of the curve at DOYs T_{mida} and T_{midb}. (c) *Autumn phenology extraction*. We adopted two widely used methods to extract EOS: (a) the date when 50% relative threshold of the annual magnitude during the decline of time series (Shen et al., 2020, 2022; White et al., 1997), (b) the date when the fastest rate of change during the decline of time series (Elmore et al., 2012), that is, T_{midb} in function 4 in step 2. To avoid systematic errors of different phenological extraction methods and make our results robust, we averaged the EOS obtained from the above-mentioned two methods as the final EOS (Peng et al., 2019; Wu et al., 2017, 2021).

For the extraction of autumn phenology from flux-tower GPP time series, the same curve fitting and phenology extraction method described above was used but only with steps 2 and 3, as flux-tower GPP had been gap filled by Marginal Distribution Sampling method (Pastorello et al., 2020).

2.5. Evaluation of Satellite-Derived Autumn Phenology Based on Ground Observations

We compared satellite-derived autumn phenology with field-observed leaf coloration and leaf fall as well as GPP-based autumn phenology. First, the two-sample *t*-test was conducted to test whether the mean difference between satellite-based EOS and in-situ autumn phenology observations was significantly different to 0. Then, the *R*-square (R^2), Mean Error (ME), Mean Absolute Error (MAE), and RMSE, were used to evaluate the satellite-based EOS based on in situ autumn phenology observations.

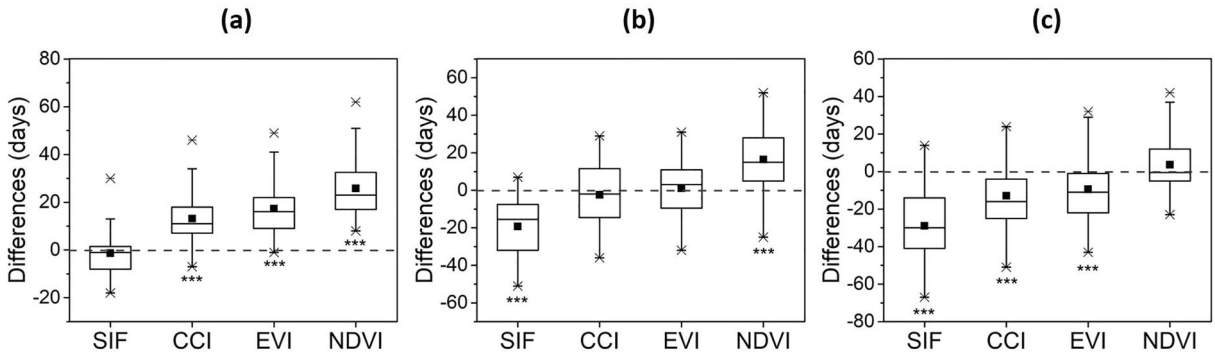

Figure 1. Boxplot of differences between autumn phenology extracted from satellite-based Solar-Induced chlorophyll Fluorescence, Chlorophyll/Carotenoid Index, Enhanced Vegetation Index, Normalized Difference Vegetation Index and flux-tower-based Gross Primary Production (a), colored leaves (b), and falling leaves (c). The student's *t*-test was conducted to test the significance of the difference, where *** represents a *p*-value less than 0.001.

3. Results

3.1. Comparison of Autumn Phenology Extracted From Different Proxies

We found that SIF-based EOS matched the best with GPP-based EOS, followed by CCI-based, EVI-based and NDVI-based ones (Figure 1a). Specifically, the SIF-based EOS was not significantly different from GPP-based EOS. EOS derived from CCI, EVI, and NDVI were instead significantly different from GPP-based EOS for a confidence interval of 99.9%, according to the two-sample *t*-test. The estimates of EOS were systematically delayed for CCI, EVI, and NDVI, and the delay was larger for NDVI than for CCI and EVI. However, EOS derived from CCI and EVI were closer to leaf coloration (both with no significant differences) than that from SIF and NDVI (Figure 1b). Compared to leaf coloration, the estimates of EOS were delayed for NDVI, but advanced for SIF. On the contrary, NDVI-based EOS matched the best with leaf fall, followed by EVI-based, CCI-based and SIF-based ones (Figure 1c). Specifically, the NDVI-based EOS had an insignificant difference with leaf fall. EOS derived from EVI, CCI, and SIF had, instead, significant difference with leaf fall for a confidence interval of 99.9%. The estimates of EOS were systematically advanced for EVI, CCI, and SIF, and the delay was larger for SIF than for CCI and EVI.

The EOS from SIF had a close relationship with that from GPP with the highest R^2 (0.331), and the smallest ME (−1.36 days), MAE (6.98 days), and RMSE (9.32 days), as shown in Table 1. The EOS of CCI followed GPP by ∼13 days, which provided an intermediate accuracy with a higher MAE (13.42) and RMSE (16.81 days) than SIF derived metrics. The EOS from EVI and NDVI lagged the GPP by ∼17 and ∼25 days respectively, especially for NDVI, which provided the highest MAE (25.79 days) and RMSE (28.26 days). The EOS from EVI was the most correlated with leaf coloration ($R^2 = 0.257$) with the lowest ME (1.07 days). The CCI-based EOS was also close to leaf coloration with a little lower ME (−2.41 days) and similar MAE (13.36) and RMSE (16.19) with EVI-based EOS. The EOS of NDVI lagged leaf coloration by ∼16 days with a higher MAE (19.85) and RMSE (24.06 days) than that of EVI, but it was the closest to leaf fall (ME = −2.93 days, MAE = 8.93 days, RMSE = 10.17). The EOS of SIF, CCI and EVI advanced the leaf fall by ∼28, ∼12, and ∼9 days respectively. The EOS from SIF was the least correlated with leaf fall ($R^2 = 0.077$) with the highest MAE (30.02 days) and RMSE (33.59 days).

3.2. Partial Correlation Between Autumn Phenology and Climate Cues

The above systematic differences between SIF, CCI, EVI, and NDVI indicated that they capture different stages of leaf senescence. In order to disentangle their underlying driving mechanisms, we compared the trajectories of satellite-based proxies with climate cues, that is, solar radiation and temperature, which are the main cues controlling leaf senescence in deciduous species in mid- and high-latitude of the Northern Hemisphere (Descals et al., 2022; Y. Zhang et al., 2020). We found that a decoupling of physiological status and structural information occurred in autumn, with asynchronous solar radiation and temperature (Figures 2a and 2b). As shown in Figure 2c, the partial correlation coefficient of SIF to solar radiation was higher than that of CCI, EVI and NDVI (0.59 vs. 0.42, 0.42, 0.27, respectively), which was a little lower than that of GPP to solar radiation ($R = 0.66$). In contrast, the partial correlation coefficient of NDVI to temperature was the highest ($R = 0.31$), followed by EVI

Table 1
Comparison Between Autumn Phenology Extracted From Satellite-Based Solar-Induced Chlorophyll Fluorescence, Chlorophyll/Carotenoid Index, Enhanced Vegetation Index, Normalized Difference Vegetation Index, and Field Observations

Field observations	Statistics	SIF-based EOS	CCI-based EOS	EVI-based EOS	NDVI-based EOS
GPP-based EOS	ME (days)	**−1.36**	13.13	17.32	25.79
	MAE (days)	**6.98**	13.42	17.35	25.79
	RMSE (days)	**9.32**	16.81	20.56	28.26
	R^2	**0.331**	0.263	0.199	0.250
Colored leaves	ME (days)	−19.30	−2.41	**1.07**	16.37
	MAE (days)	20.11	13.36	**12.70**	19.58
	RMSE (days)	25.15	16.19	**15.80**	24.06
	R^2	0.216	0.220	**0.257**	0.155
Falling leaves	ME (days)	−28.96	−12.94	−9.45	**3.66**
	MAE (days)	30.02	17.10	16.27	**11.30**
	RMSE (days)	33.59	19.84	19.32	**15.44**
	R^2	0.077	0.248	0.131	**0.277**

Note. Statistics of the comparisons (mean error [ME], mean absolute error [MAE], root mean square error [RMSE], and R-square [R^2]) are reported. Values in bold highlight the highest R^2 and smallest deviation from satellite-based SIF, CCI, EVI, NDVI, and field observations.

($R = 0.30$), CCI ($R = 0.16$) and SIF ($R = 0.06$). To confirm the robustness of the analysis, we further test the sensitivity of satellite proxies (i.e., GPP, SIF, CCI, EVI, and NDVI) to climate cues (see Table S3 in Supporting Information S1). We found that the sensitivity of NDVI, EVI, CCI, SIF, and GPP to solar radiation in autumn was increased sequentially, while it was decreased in sequence to temperature. In summary, the sequence among the autumn phenology derived from different satellite proxies was consistent with their responses to climate cues, where SIF had the highest partial correlation coefficient to solar radiation in autumn, followed by CCI, EVI, and NDVI, while NDVI was more correlated with temperature, followed by EVI, CCI, and SIF.

4. Discussion

4.1. Mechanism Analysis of Divergence in Autumn Phenology Extracted From Different Satellite Proxies

Autumn phenology has been increasingly studied with varied satellite proxies (Jeong et al., 2017; Liu et al., 2016; Lu et al., 2018; C. Wang et al., 2023; Yin et al., 2020), however, the autumn phenology derived by different satellite proxies were divergent. In this study, we compared autumn phenology extracted from different satellite proxies with field observations at deciduous forest sites. The sequence among the autumn phenology derived from different satellite proxies was highlighted in this study, where SIF-based autumn phenology was the earliest, followed by CCI-based, EVI-based and NDVI-based autumn phenology. Some recent studies have presented that SIF-based EOS is close to GPP-based EOS (Jeong et al., 2017; Lu et al., 2018; C. Wang et al., 2019), but is significantly earlier than the green biomass decrease proxied by EVI or NDVI (D'Odorico et al., 2015; Walther et al., 2016; C. Wang et al., 2022; Yang et al., 2022), which are consistent with our findings. In addition, we found the newly emerged physiological index CCI performed between SIF and EVI, demonstrating its potential for estimating GPP-derived EOS for deciduous forests (Yin et al., 2020), but not as good as SIF.

The timing of leaf senescence is likely to be a trade-off between photosynthetic carbon assimilation and autumnal nutrient resorption at different stages in the seasonal functioning of leaves (Fracheboud et al., 2009; Keskitalo et al., 2005). When trees reach their maximum carbon storage capacity, they will initialize nutrient resorption and senescence (Chen et al., 2021). The photosynthetic carbon assimilation reflects photosynthesis activity which is mainly controlled by photoperiod and radiation (Descals et al., 2022; Y. Zhang et al., 2020). The initial stage of leaf senescence is a decrease in photosynthetic activity due to decreasing incoming radiation (Chen et al., 2021; Y. Zhang et al., 2020). SIF, as a direct and effective proxy for photosynthesis by way of complex mechanisms of energy dissipation (Porcar-Castell et al., 2014; Y. G. Zhang et al., 2014), decreased the earliest in autumn (Joiner et al., 2011), followed by leaf nutrient relocation and chlorophyll degradation (Marien et al., 2019), when leaves

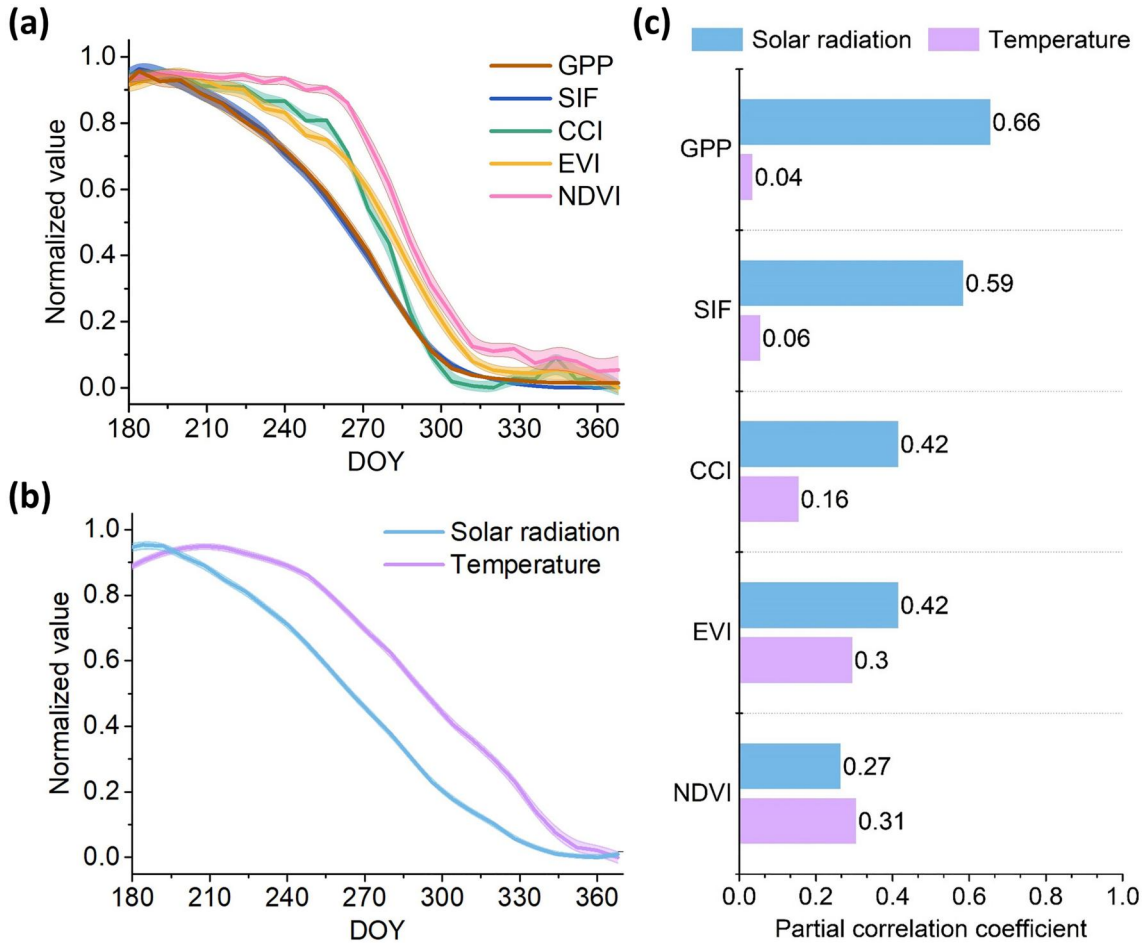

Figure 2. Relationship between satellite proxies and climatic factors at all available fluxnet sites in the second half of the year. Time series of multi-year mean (dots) and standard error (shaded area) values of flux-tower-based Gross Primary Production (GPP) and satellite-based Solar-Induced chlorophyll Fluorescence (SIF), Chlorophyll/Carotenoid Index (CCI), Enhanced Vegetation Index (EVI), and Normalized Difference Vegetation Index (NDVI) (a), and solar radiation and temperature (b). Partial correlation coefficients between GPP, SIF, CCI, EVI, and NDVI with solar radiation and temperature (c).

undergo to recover valuable elements contained in their pigments (Estiarte et al., 2023). Thus, CCI decreased a little later than SIF as it tracks chlorophyll decomposition (Gamon et al., 2016). The chlorophyll degradation progressively leads to the leaf coloration as other non-green pigments, such as carotenoids, become visible (Croft & Chen, 2018; Feild et al., 2001). CCI can also track leaf coloration since carotenoids are involved. In fact, CCI is the index more correlated to leaf coloration after EVI, as chlorophyll degradation and leaf coloration are interrelated, resulting in similar performance between CCI and EVI in autumn phenology derivation. At the end of the leaf senescence process, nutrient transport through the phloem is stopped by the formation of an abscission and separation layer in the petiole, which leads to leaf coloration, and finally leaf fall (Fracheboud et al., 2009; Keskitalo et al., 2005; Ruttink et al., 2007).

4.2. Limitations, Uncertainties, and Future Outlook

The SIF time series utilized in this study were obtained from the spatially and temporally continuous GOSIF product, which was generated by a predictive SIF model using the MODIS EVI and meteorological reanalysis data as inputs. This ensured that the autumn phenology could be generated by continuous SIF time series, but the uncertainty in SIF estimates from the predictive model and data sources (e.g., the meteorological reanalysis data, biases in EVI) would inevitably introduce to the phenological extraction. Furthermore, it should be noted that the autumn phenology in this study was derived from 0.05° and 8-day composite satellite data, whereas ground observations relied on daily point-based measurements. Although studied sites are representative for each station and the surrounding area, mismatches between satellite-based phenology and ground-based observations at both

temporal and spatial scales are unavoidable (Helman, 2018; X. Zhang et al., 2006). Future applications of satellite proxies (especially for satellite SIF) in phenological studies will further benefit from the next generation of sensor development with higher spatial and/or temporal resolutions. (e.g., downscaling the current SIF products, launching new satellites, etc.). Besides, another limitation of this study is that we could not directly validate whether CCI captures the timing of chlorophyll degradation because of the lack of such field measurements. More dedicated experiments integrating field campaigns and satellite observations are warranted to further validate our hypothesis with in situ time series of leaf photosynthetic rate, chlorophyll content and leaf area index. Moreover, the performances of different satellite proxies in different ecosystem types (e.g., grasslands or croplands) should be further explored.

This study revealed the sequence of the autumn phenology extracted from different satellite proxies, that is, SIF < CCI < EVI < NDVI, and explained this interesting phenomenon in terms of leaf senescence timetable captured by them. The capacity of CCI to capture chlorophyll degradation has been demonstrated by in situ measurements (Gamon et al., 2016; Wong et al., 2019). This study, furthermore, provided empirical evidence that SIF, EVI and NDVI also capture complementary stages of the progressive leaf senescence process. Specifically, the autumn phenology extracted from SIF corresponds with the attenuation of photosynthetic activity, while EVI is prone to track leaf color changes from greenness perspective (X. Zhang, 2015), and NDVI is more sensitive to structural changes such as leaf fall (Hashemi & Chai, 2013; Nagai et al., 2010). This indicated that the neglect of the specific definition of different satellite proxies is one of the main reasons resulting in diverse satellite-derived autumn phenology. Therefore, it is suggested that the definition of the phenology metrics derived from different satellite proxies should be carefully considered for a correct interpretation of autumn phenology. In addition, we found that the divergent autumn phenology derived by different satellite proxies was contributed to their different responses to asynchronous solar radiation and temperature in autumn. The partial correlation analysis and sensitivity test between autumn phenology and environmental cues further supported this foliar senescence timetable. It should be noticed that autumn phenology would also be affected by extreme climate events with uncertainty (e.g., heat, flood, and drought) (Li & Xiao, 2020; Yoshida et al., 2015). Future work should take into account that autumn phenology derived by different satellite proxies have different responses to climate/environmental factors under different levels of stress, to better promote satellite-based autumn phenology applications in different usage scenarios.

5. Conclusion

This study compared the autumn phenology extracted from satellite-based SIF, CCI, EVI, and NDVI in deciduous forests with ground observations, and explored the underlying mechanisms by analyzing their responses to climatic conditions in autumn. We highlighted that leaf senescence over deciduous forests is a progressive process following a specific timetable, and autumn phenology derived from SIF, CCI, EVI, and NDVI successfully capture the sequential attenuation of photosynthetic activity, chlorophyll degradation, leaf coloration, and leaf fall, respectively. These findings help to improve our interpretation of land surface phenology. We suggest that the definition of the phenology metrics derived from different satellite proxies should be carefully considered for a correct interpretation of autumn phenology, to better promote satellite-based autumn phenology applications in different usage scenarios.

Acknowledgments
This research was funded by the National Natural Science Foundation of China (42101391 and 41971282), the Sichuan Science and Technology Program (2021JDJQ0007), the Spanish Government Grants PID2019-110521GB-I00 and TED2021-132627B-I00, the Fundación Ramón Areces Grant CIVP20A6621, the Catalan Government Grant SGR2017-1005, the Fundamental Research Funds for the Central Universities (CCNU22QN019), and the China Postdoctoral Science Foundation (2021M701361 and 2023T160254). This work represents a contribution to CSIC Interdisciplinary Thematic Platform Teledetección (PTI-TELEDETECT).

Data Availability Statement

The pre-processed data is openly available (C. Wang, 2024). The data includes phenological observations at selected NPN sites, GPP observations with an interval of 8 days at selected Fluxnet sites, climate reanalysis data and satellite-extracted vegetation proxies (i.e., SIF, CCI, EVI, and NDVI) at an 8-day interval across those sites.

References

Bonan, G. B. (2008). Forests and climate change: Forcings, feedbacks, and the climate benefits of forests. *Science*, *320*(5882), 1444–1449. https://doi.org/10.1126/science.1155121

Chen, L., Rossi, S., Smith, N. G., & Liu, J. (2021). Shifts in leaf senescence across the Northern Hemisphere in response to seasonal warming (p. 453498).

Croft, H., & Chen, J. M. (2018). Leaf pigment content. In S. Liang (Ed.), *Comprehensive remote sensing* (pp. 117–142). Elsevier.

Croft, H., Chen, J. M., Luo, X., Bartlett, P., Chen, B., & Staebler, R. M. (2017). Leaf chlorophyll content as a proxy for leaf photosynthetic capacity. *Global Change Biology*, *23*(9), 3513–3524. https://doi.org/10.1111/gcb.13599

Descals, A., Verger, A., Yin, G., Filella, I., Fu, Y. H., Piao, S., et al. (2022). Radiation-constrained boundaries cause nonuniform responses of the carbon uptake phenology to climatic warming in the Northern Hemisphere. *Global Change Biology*, *00*(3), 1–12. https://doi.org/10.1111/gcb.16502

D'Odorico, P., Gonsamo, A., Gough, C. M., Bohrer, G., Morison, J., Wilkinson, M., et al. (2015). The match and mismatch between photosynthesis and land surface phenology of deciduous forests. *Agricultural and Forest Meteorology*, *214–215*, 25–38. https://doi.org/10.1016/j.agrformet.2015.07.005

Elmore, A. J., Guinn, S. M., Minsley, B. J., & Richardson, A. D. (2012). Landscape controls on the timing of spring, autumn, and growing season length in mid-Atlantic forests. *Global Change Biology*, *18*(2), 656–674. https://doi.org/10.1111/j.1365-2486.2011.02521.x

Estiarte, M., Campiolli, M., Mayol, M., & Penuelas, J. (2023). Variability and limits in resorption of nitrogen and phosphorus during foliar senescence. *Plant Communications*, *4*(2). https://doi.org/10.1016/j.xplc.2022.100503

Estiarte, M., & Penuelas, J. (2015). Alteration of the phenology of leaf senescence and fall in winter deciduous species by climate change: Effects on nutrient proficiency. *Global Change Biology*, *21*(3), 1005–1017. https://doi.org/10.1111/gcb.12804

Feild, T. S., Lee, D. W., & Holbrook, N. M. (2001). Why leaves turn red in autumn. The role of anthocyanins in senescing leaves of red-osier dogwood. *Plant Physiology*, *127*(2), 566–574. https://doi.org/10.1104/pp.127.2.566

Fracheboud, Y., Luquez, V., Björkén, L., Sjödin, A., Tuominen, H., & Jansson, S. (2009). The control of autumn senescence in European Aspen. *Plant Physiology*, *149*(4), 1982–1991. https://doi.org/10.1104/pp.108.133249

Gallinat, A. S., Primack, R. B., & Wagner, D. L. (2015). Autumn, the neglected season in climate change research. *Trends in Ecology & Evolution*, *30*(3), 169–176. https://doi.org/10.1016/j.tree.2015.01.004

Gamon, J. A., Field, C. B., Goulden, M. L., Griffin, K. L., Hartley, A. E., Joel, G., et al. (1995). Relationships between NDVI, canopy structure, and photosynthesis in three Californian vegetation types. *Ecological Applications*, *5*(1), 28–41. https://doi.org/10.2307/1942049

Gamon, J. A., Huemmrich, K. F., Wong, C. Y. S., Ensminger, I., Garrity, S., Hollinger, D. Y., et al. (2016). A remotely sensed pigment index reveals photosynthetic phenology in evergreen conifers. *Proceedings of the National Academy of Sciences of the United States of America*, *113*(46), 13087–13092. https://doi.org/10.1073/pnas.1606162113

Ganguly, S., Friedl, M. A., Tan, B., Zhang, X., & Verma, M. (2010). Land surface phenology from MODIS: Characterization of the collection 5 global land cover dynamics product. *Remote Sensing of Environment*, *114*(8), 1805–1816. https://doi.org/10.1016/j.rse.2010.04.005

Guyon, D., Guillot, M., Vitasse, Y., Cardot, H., Hagolle, O., Delzon, S., & Wigneron, J. P. (2011). Monitoring elevation variations in leaf phenology of deciduous broadleaf forests from SPOT/VEGETATION time-series. *Remote Sensing of Environment*, *115*(2), 615–627. https://doi.org/10.1016/j.rse.2010.10.006

Hashemi, S. A., & Chai, M. M. F. (2013). Investigation of NDVI in relation to the growth phases of beech leaves in forest. *Arabian Journal of Geosciences*, *6*(9), 3341–3347. https://doi.org/10.1007/s12517-012-0565-y

Helman, D. (2018). Land surface phenology: What do we really 'see' from space? *Science of the Total Environment*, *618*, 665–673. https://doi.org/10.1016/j.scitotenv.2017.07.237

Huete, A., Didan, K., Miura, T., Rodriguez, E., Gao, X., & Ferreira, L. (2002). Overview of the radiometric and biophysical performance of the MODIS vegetation indices. *Remote Sensing of Environment*, *83*(1–2), 195–213. https://doi.org/10.1016/s0034-4257(02)00096-2

Jeong, S.-J., Schimel, D., Frankenberg, C., Drewry, D. T., Fisher, J. B., Verma, M., et al. (2017). Application of satellite solar-induced chlorophyll fluorescence to understanding large-scale variations in vegetation phenology and function over northern high latitude forests. *Remote Sensing of Environment*, *190*, 178–187. https://doi.org/10.1016/j.rse.2016.11.021

Joiner, J., Yoshida, Y., Vasilkov, A. P., Yoshida, Y., Corp, L. A., & Middleton, E. M. (2011). First observations of global and seasonal terrestrial chlorophyll fluorescence from space. *Biogeosciences*, *8*(3), 637–651. https://doi.org/10.5194/bg-8-637-2011

Keskitalo, J., Bergquist, G., Gardestrom, P., & Jansson, S. (2005). A cellular timetable of autumn senescence. *Plant Physiology*, *139*(4), 1635–1648. https://doi.org/10.1104/pp.105.066845

Le Quere, C., Raupach, M. R., Canadell, J. G., Marland, G., Bopp, L., Ciais, P., et al. (2009). Trends in the sources and sinks of carbon dioxide. *Nature Geoscience*, *2*(12), 831–836. https://doi.org/10.1038/ngeo689

Li, X., & Xiao, J. (2019). A global, 0.05-degree product of solar-induced chlorophyll fluorescence derived from OCO-2, MODIS, and reanalysis data. *Remote Sensing*, *11*(5), 517. https://doi.org/10.3390/rs11050517

Li, X., & Xiao, J. (2020). Global climatic controls on interannual variability of ecosystem productivity: Similarities and differences inferred from solar-induced chlorophyll fluorescence and enhanced vegetation index. *Agricultural and Forest Meteorology*, 288–289.

Liu, Q., Fu, Y. H., Zhu, Z., Liu, Y., Liu, Z., Huang, M., et al. (2016). Delayed autumn phenology in the Northern Hemisphere is related to change in both climate and spring phenology. *Global Change Biology*, *22*(11), 3702–3711. https://doi.org/10.1111/gcb.13311

Lu, X., Liu, Z., Zhou, Y., Liu, Y., & Tang, J. (2018). Comparison of phenology estimated from reflectance-based indices and solar-induced chlorophyll fluorescence (SIF) observations in a temperate forest using GPP-based phenology as the standard. *Remote Sensing*, *10*(6), 932. https://doi.org/10.3390/rs10060932

Lyapustin, A., Wang, Y., Laszlo, I., & Korkin, S. (2012). Improved cloud and snow screening in MAIAC aerosol retrievals using spectral and spatial analysis. *Atmospheric Measurement Techniques*, *5*(4), 843–850. https://doi.org/10.5194/amt-5-843-2012

Marien, B., Balzarolo, M., Dox, I., Leys, S., Lorène, M. J., Geron, C., et al. (2019). Detecting the onset of autumn leaf senescence in deciduous forest trees of the temperate zone. *New Phytologist*, *224*(1), 166–176. https://doi.org/10.1111/nph.15991

Middleton, E. M., Huemmrich, K., Landis, D., Black, T., Barr, A., & McCaughey, J. (2016). Photosynthetic efficiency of northern forest ecosystems using a MODIS-derived Photochemical Reflectance Index (PRI). *Remote Sensing of Environment*, *187*, 345–366. https://doi.org/10.1016/j.rse.2016.10.021

Munoz-Sabater, J., Dutra, E., Agustí-Panareda, A., Albergel, C., Arduini, G., Balsamo, G., et al. (2021). ERA5-Land: A state-of-the-art global reanalysis dataset for land applications. *Earth System Science Data*, *13*(9), 4349–4383. https://doi.org/10.5194/essd-13-4349-2021

Myneni, R. B., Hall, F. G., Sellers, P. J., & Marshak, A. L. (1995). The interpretation of spectral vegetation indexes. *IEEE Transactions on Geoscience and Remote Sensing*, *33*(2), 481–486. https://doi.org/10.1109/36.377948

Nagai, S., Nasahara, K. N., Muraoka, H., Akiyama, T., & Tsuchida, S. (2010). Field experiments to test the use of the normalized-difference vegetation index for phenology detection. *Agricultural and Forest Meteorology*, *150*(2), 152–160. https://doi.org/10.1016/j.agrformet.2009.09.010

Pastorello, G., Trotta, C., Canfora, E., Chu, H., Christianson, D., Cheah, Y. W., et al. (2020). The FLUXNET2015 dataset and the ONEFlux processing pipeline for eddy covariance data. *Scientific Data*, *7*(1), 225. https://doi.org/10.1038/s41597-020-0534-3

Peng, J., Wu, C., Zhang, X., Wang, X., & Gonsamo, A. (2019). Satellite detection of cumulative and lagged effects of drought on autumn leaf senescence over the Northern Hemisphere. *Global Change Biology*, *118*(16), e2015821118. https://doi.org/10.1111/gcb.14627

Penuelas, J., Gamon, J. A., Fredeen, A. L., Merino, J., & Field, C. B. (1994). Reflectance indexes associated with physiological-changes in nitrogen-limited and water-limited sunflower leaves. *Remote Sensing of Environment*, *48*(2), 135–146. https://doi.org/10.1016/0034-4257(94)90136-8

Porcar-Castell, A., Tyystjärvi, E., Atherton, J., van der Tol, C., Flexas, J., Pfündel, E. E., et al. (2014). Linking chlorophyll a fluorescence to photosynthesis for remote sensing applications: Mechanisms and challenges. *Journal of Experimental Botany*, *65*(15), 4065–4095. https://doi.org/10.1093/jxb/eru191

Ren, P., Liu, Z., Zhou, X., Peng, C., Xiao, J., Wang, S., et al. (2021). Strong controls of daily minimum temperature on the autumn photosynthetic phenology of subtropical vegetation in China. *Forest Ecosystems*, *8*(1), 31. https://doi.org/10.1186/s40663-021-00309-9

Richardson, A. D., Andy Black, T., Ciais, P., Delbart, N., Friedl, M. A., Gobron, N., et al. (2010). Influence of spring and autumn phenological transitions on forest ecosystem productivity. *Philosophical Transactions of the Royal Society B: Biological Sciences*, *365*(1555), 3227–3246. https://doi.org/10.1098/rstb.2010.0102

Ruttink, T., Arend, M., Morreel, K., Storme, V., Rombauts, S., Fromm, J., et al. (2007). A molecular timetable for apical bud formation and dormancy induction in poplar. *The Plant Cell*, *19*(8), 2370–2390. https://doi.org/10.1105/tpc.107.052811

Shen, M., Jiang, N., Peng, D., Rao, Y., Huang, Y., Fu, Y. H., et al. (2020). Can changes in autumn phenology facilitate earlier green-up date of northern vegetation? *Agricultural and Forest Meteorology*, *291*, 108077. https://doi.org/10.1016/j.agrformet.2020.108077

Shen, M., Zhu, X., Peng, D., Jiang, N., Huang, Y., Chen, J., et al. (2022). Greater temperature sensitivity of vegetation greenup onset date in areas with weaker temperature seasonality across the Northern Hemisphere. *Agricultural and Forest Meteorology*, *313*, 108759. https://doi.org/10.1016/j.agrformet.2021.108759

Walther, S., Voigt, M., Thum, T., Gonsamo, A., Zhang, Y., Köhler, P., et al. (2016). Satellite chlorophyll fluorescence measurements reveal large-scale decoupling of photosynthesis and greenness dynamics in boreal evergreen forests. *Global Change Biology*, *22*(9), 2979–2996. https://doi.org/10.1111/gcb.13200

Wang, C. (2024). Filed-observed autumn phenology and satellite variables [Dataset]. Zenodo. https://doi.org/10.5281/zenodo.10546309

Wang, C., Beringer, J., Hutley, L. B., Cleverly, J., Li, J., Liu, Q., & Sun, Y. (2019). Phenology dynamics of dryland ecosystems along the North Australian tropical transect revealed by satellite solar-induced chlorophyll fluorescence. *Geophysical Research Letters*, *46*(10), 5294–5302. https://doi.org/10.1029/2019gl082716

Wang, C., Chen, Y., Tong, W., Zhou, W., Li, J., Xu, B., & Hu, Q. (2023). Mapping crop phenophases in reproductive growth period by satellite solar-induced chlorophyll fluorescence: A case study in mid-temperate zone in China. *ISPRS Journal of Photogrammetry and Remote Sensing*, *205*, 191–205. https://doi.org/10.1016/j.isprsjprs.2023.10.005

Wang, C., Wu, Y., Hu, Q., Hu, J., Chen, Y., Lin, S., & Xie, Q. (2022). Comparison of vegetation phenology derived from solar-induced chlorophyll fluorescence and enhanced vegetation index, and their relationship with climatic limitations. *Remote Sensing*, *14*(13), 3018. https://doi.org/10.3390/rs14133018

Wang, R., Gamon, J. A., Emmerton, C. A., Springer, K. R., Yu, R., & Hmimina, G. (2020). Detecting intra- and inter-annual variability in gross primary productivity of a North American grassland using MODIS MAIAC data. *Agricultural and Forest Meteorology*, *281*, 107859. https://doi.org/10.1016/j.agrformet.2019.107859

Wang, X., Dannenberg, M. P., Yan, D., Jones, M. O., Kimball, J. S., Moore, D. J., et al. (2020). Globally consistent patterns of asynchrony in vegetation phenology derived from optical, microwave, and fluorescence satellite data. *Journal of Geophysical Research: Biogeosciences*, *125*(7), e2020JG005732. https://doi.org/10.1029/2020jg005732

White, M. A., Thornton, P. E., & Running, S. W. (1997). A continental phenology model for monitoring vegetation responses to interannual climatic variability. *Global Biogeochemical Cycles*, *11*(2), 217–234. https://doi.org/10.1029/97gb00330

Wong, C. Y. S., D'Odorico, P., Bhathena, Y., Arain, M. A., & Ensminger, I. (2019). Carotenoid based vegetation indices for accurate monitoring of the phenology of photosynthesis at the leaf-scale in deciduous and evergreen trees. *Remote Sensing of Environment*, *233*, 111407. https://doi.org/10.1016/j.rse.2019.111407

Wong, C. Y. S., & Gamon, J. A. (2015). Three causes of variation in the photochemical reflectance index (PRI) in evergreen conifers. *New Phytologist*, *206*(1), 187–195. https://doi.org/10.1111/nph.13159

Wu, C., Chen, J. M., Black, T. A., Price, D. T., Kurz, W. A., Desai, A. R., et al. (2013). Interannual variability of net ecosystem productivity in forests is explained by carbon flux phenology in autumn. *Global Ecology and Biogeography*, *22*(8), 994–1006. https://doi.org/10.1111/geb.12044

Wu, C., Peng, D., Soudani, K., Siebicke, L., Gough, C. M., Arain, M. A., et al. (2017). Land surface phenology derived from normalized difference vegetation index (NDVI) at global FLUXNET sites. *Agricultural and Forest Meteorology*, *233*, 171–182. https://doi.org/10.1016/j.agrformet.2016.11.193

Wu, C., Wang, J., Ciais, P., Peñuelas, J., Zhang, X., Sonnentag, O., et al. (2021). Widespread decline in winds delayed autumn foliar senescence over high latitude. *Proceedings of the National Academy of Sciences of the United States of America*, *118*(16), e2015821118. https://doi.org/10.1073/pnas.2015821118

Yang, Y., Chen, R., Yin, G., Wang, C., Liu, G., Verger, A., et al. (2022). Divergent performances of vegetation indices in extracting photosynthetic phenology for northern deciduous broadleaf forests. *IEEE Geoscience and Remote Sensing Letters*, *19*, 1–5. https://doi.org/10.1109/lgrs.2022.3182405

Yin, G., Verger, A., Descals, A., Filella, I., & Peñuelas, J. (2022). A broadband green-red vegetation index for monitoring gross primary production phenology. *Journal of Remote Sensing*, *2022*, 1–10. https://doi.org/10.34133/2022/9764982

Yin, G., Verger, A., Filella, I., Descals, A., & Penuelas, J. (2020). Divergent estimates of forest photosynthetic phenology using structural and physiological vegetation indices. *Geophysical Research Letters*, *47*(18), e2020GL089167. https://doi.org/10.1029/2020gl089167

Yoshida, Y., Joiner, J., Tucker, C., Berry, J., Lee, J. E., Walker, G., et al. (2015). The 2010 Russian drought impact on satellite measurements of solar-induced chlorophyll fluorescence: Insights from modeling and comparisons with parameters derived from satellite reflectances. *Remote Sensing of Environment*, *166*, 163–177. https://doi.org/10.1016/j.rse.2015.06.008

Zhang, J., Xiao, J., Tong, X., Zhang, J., Meng, P., Li, J., et al. (2022). NIRv and SIF better estimate phenology than NDVI and EVI: Effects of spring and autumn phenology on ecosystem production of planted forests. *Agricultural and Forest Meteorology*, *315*, 108819. https://doi.org/10.1016/j.agrformet.2022.108819

Zhang, X. (2015). Reconstruction of a complete global time series of daily vegetation index trajectory from long-term AVHRR data. *Remote Sensing of Environment*, *156*, 457–472. https://doi.org/10.1016/j.rse.2014.10.012

Zhang, X., Friedl, M. A., & Schaaf, C. B. (2006). Global vegetation phenology from Moderate Resolution Imaging Spectroradiometer (MODIS): Evaluation of global patterns and comparison with in situ measurements. *Geophysical Research Bulletin*, *111*(G4), G04017. https://doi.org/10.1029/2006JG000217

Zhang, Y., Commane, R., Zhou, S., Williams, A. P., & Gentine, P. (2020). Light limitation regulates the response of autumn terrestrial carbon uptake to warming. *Nature Climate Change*, *10*(8), 739–743. https://doi.org/10.1038/s41558-020-0806-0

Zhang, Y. G., Guanter, L., Berry, J. A., Joiner, J., van der Tol, C., Huete, A., et al. (2014). Estimation of vegetation photosynthetic capacity from space-based measurements of chlorophyll fluorescence for terrestrial biosphere models. *Global Change Biology*, *20*(12), 3727–3742. https://doi.org/10.1111/gcb.12664

Zheng, J., Ge, Q., & Hao, Z. (2002). The influence of climate warming on plant phenology change in China in recent 40 years. *Chinese Science Bulletin*, *47*(20), 1582–1587.